

Geometric magnetism and new enantio-sensitive observables in photoionization of chiral molecules

Andres F. Ordonez^{1,2}, David Ayuso^{1,3}, Piero Decleva^{4,5} and Olga Smirnova^{1,6}

¹*Max-Born-Institut, Max-Born-Str. 2A, 12489 Berlin, Germany*

²*ICFO-Institut de Ciències Fotoniques,
The Barcelona Institute of Science and Technology,
08860 Castelldefels (Barcelona), Spain*

³*Department of Physics, Imperial College London,
SW7 2BW London, United Kingdom*

⁴*Dipartimento di Scienze Chimiche e Farmaceutiche,
Università degli Studi di Trieste, Trieste, Italy*

⁵*CNR-IOM DEMOCRITOS, Trieste, Italy*

⁶*Technische Universität Berlin,
Straße des 17. Juni 135, 10623 Berlin, Germany*

(Dated: March 23, 2022)

Abstract

Chiral molecules are instrumental for molecular recognition in living organisms. Distinguishing between two opposite enantiomers, the mirror twins of the same chiral molecule, is both vital and challenging. Photoelectron circular dichroism (PECD), an extremely sensitive probe of molecular chirality via photoionization, outperforms standard optical methods by many orders of magnitude. Here we show that the physical origin of PECD in chiral molecules is linked to the concept of geometric magnetism, which enables a broad class of phenomena in solids including the anomalous electron velocity, the Hall effect, and related topological phenomena. We uncover the geometric field in molecular photoionization, which leads to a new class of enantio-sensitive observables emerging due to ultrafast excitation of chiral electronic or vibronic currents prior to ionization. Next, we introduce the first member of this new class: enantio-sensitive orientation of chiral molecules via photoionization. This effect opens new routes to both enantio-separation and imaging of chiral dynamics on ultrafast time scales. Our work suggests that geometric fields in photoionization provide the bridge between the two geometrical properties, chirality and topology.

Chiral molecules are characterised by their handedness, an extra degree of freedom of a purely geometrical origin. Geometrical properties in real space are determined by the nuclear configuration in molecules or by the lattice configuration in solids. In solids, they map onto geometrical or topological properties of Hilbert space vectors, leading to robust observables associated with the electronic response to electromagnetic fields and new, topological, phases of matter. Geometric magnetism, introduced by M. Berry [1], is a key concept underlying these phenomena. One of the manifestations of geometric magnetism is the Berry curvature in solids, which enables a class of new observables in condensed matter systems related to the so-called anomalous electron velocity imparted by the Berry curvature [2].

We show that similar geometric magnetic fields and “anomalous” observables induced by such fields also arise in one[3–7]– or multiphoton[8–10] ionization of chiral molecules by circularly polarized fields, with photoelectron circular dichroism (PECD)[3–5] being one example of such “anomalous” phenomena. The PECD signal is encoded in the direction of the net photoelectron current, which is opposite in opposite enantiomers and is perpendicular to the light polarization plane. Unlike standard absorption circular dichroism (CD), PECD arises already in the electric-dipole approximation and is associated with very strong enantio-sensitive signals.

We show that not only the emergence and enantio-sensitivity of PECD is linked to the concept of geometric magnetism, but that this concept also allows one to predict new efficient enantio-sensitive

observables. One of them is enantio-sensitive orientation of chiral molecules via two- or multi-photon ionization, which we call “molecular orientation circular dichroism” (MOCD). Crucially, these new observables rely on ultrafast excitation of chiral electronic or vibronic currents, linking geometric magnetism to yet another important concept in ultrafast science: the concept of charge-directed reactivity.

Charge directed chemical reactivity [11] implies that ultrafast electron dynamics can affect the outcome of chemical reactions, opening an important direction in attochemistry [12–18]. We show that ultrafast electron currents can lead to opposite orientation of left and right enantiomers of the same molecule upon photoionization by circularly polarized light, thus presenting an example of enantio-sensitive charge-directed reactivity, with geometric magnetism providing a platform for its description.

Geometric magnetism: molecules vs solids

Geometric magnetism in photoionization of chiral molecules with circularly polarized light originates from the so-called propensity field, which we have introduced recently [19]. It emerges in photoionization of randomly oriented molecules and involves the vector product of two conjugated photoionization dipoles (\vec{d}_{kg} in the length or \vec{p}_{kg} in the velocity gauges):

$$\vec{B}(\vec{k}) = i[\vec{d}_{kg} \times \vec{d}_{kg}^*] = i \frac{[\vec{p}_{kg} \times \vec{p}_{kg}^*]}{(E_k - E_g)^2}. \quad (1)$$

Here $E_k = k^2/2$ is the photoelectron energy and E_g is the energy of the initial (e.g. ground) state. The field $\vec{B}(\vec{k})$ is a molecular-frame property.

The second equality in Eq. (1) is also true for the Berry curvature in a two-band solid [20]:

$$\vec{\Omega}(\vec{k}) = i \frac{[\vec{p}_k^{vc} \times \vec{p}_k^{vc*}]}{(E_c - E_v)^2}, \quad (2)$$

where the matrix elements \vec{p}^{vc} and energies $E_{v,c}$ describe transitions between the valence (v) and conduction (c) bands. Just like the Berry curvature (Eq. (2)) characterises \vec{k} -dependent circular dichroism in interband transitions in solids[20], the propensity field (Eq. (1)) characterises \vec{k} -dependent circular dichroism in photoionization[19].

The analogy between $\vec{B}(\vec{k})$ [Eq. (1)] and $\vec{\Omega}(\vec{k})$ [Eq. (2)] runs deep. The enantio-sensitive photoionization current in molecules (PECD), is orthogonal to the polarization plane of the driving laser light,

and can be written via the enantio-sensitive and k -dependent conductivity $\sigma_{zz}(k)$ as

$$j_z(k) = \sigma_{zz}[\vec{E}_\omega \times \vec{E}_\omega^*]_z. \quad (3)$$

where[21] $\sigma_{zz}(k)$ is proportional to the flux of the field $\vec{B}(\vec{k})$ [Eq. (1)] through the sphere in \vec{k} -space with radius $k = \sqrt{2E}$ and the surface element $d\vec{S} = k^2 d\Theta_k(\vec{k}/k)$, where $d\Theta_k \equiv d\phi_k d\theta_k \sin \theta_k$:

$$\sigma_{zz}(k) = \frac{1}{6k} \oint \vec{B}(\vec{k}) \cdot d\vec{S}. \quad (4)$$

The solid state analogue to PECD is the circular photogalvanic effect in non-inversion-symmetric solids: circularly polarized light induces net electron current perpendicular to its polarization plane. This current has recently been related [22] to the Berry curvature $\vec{\Omega}(\vec{k})$ as[23]

$$\vec{j}_z(k) = \sigma_{zz}[\vec{E}_\omega \times \vec{E}_\omega^*]_z, \quad (5)$$

$$\sigma_{zz}(k) = \frac{e^3}{6h^2} \oint \vec{\Omega}(\vec{k}) \cdot d\vec{S}. \quad (6)$$

Eq. (6) is exact in the two-band approximation. The similarity between Eqs. (5,6) and (3,4) is clear.

In photoionization from a superposition of two states $|j\rangle + e^{-i\phi_{ij}}|i\rangle$ ($\phi_{ij} = \omega_{ij}t$, with $\omega_{ij} \equiv \omega_i - \omega_j$ being the transition frequency between the states) the propensity field acquires an additional term, which encodes the coherence between the excited states:

$$\vec{B}_{ij}(\vec{k}, \phi_{ij}) = -\frac{1}{2}i \left[\vec{d}_{ki}^* \times \vec{d}_{kj} \right] e^{i\phi_{ij}} + \text{c.c.} \equiv \vec{Q}_{ij}(\vec{k}) \cos \phi_{ij} + \vec{P}_{ij}(\vec{k}) \sin \phi_{ij}, \quad (7)$$

where we have introduced the displacement $\vec{Q}_{ij}(\vec{k})$ and current $\vec{P}_{ij}(\vec{k})$ quadratures:

$$\vec{Q}_{ij}(\vec{k}) \equiv -\Re \left\{ i \left[\vec{d}_{ki}^* \times \vec{d}_{kj} \right] \right\}, \quad (8)$$

$$\vec{P}_{ij}(\vec{k}) \equiv \Im \left\{ i \left[\vec{d}_{ki}^* \times \vec{d}_{kj} \right] \right\}. \quad (9)$$

Examples of the displacement $\vec{Q}_{ij}(\vec{k})$ and current $\vec{P}_{ij}(\vec{k})$ quadratures for a coherent superposition of $i=\text{LUMO}$ and $j=\text{LUMO}+1$ in propylene oxide (a chiral molecule) are shown in Fig. 1. Eq. (7) describes the geometric field oscillating at the frequency ω_{ij} . For $i = j = g$, $\phi_{ij} = 0$ and Eq. (7) reduces

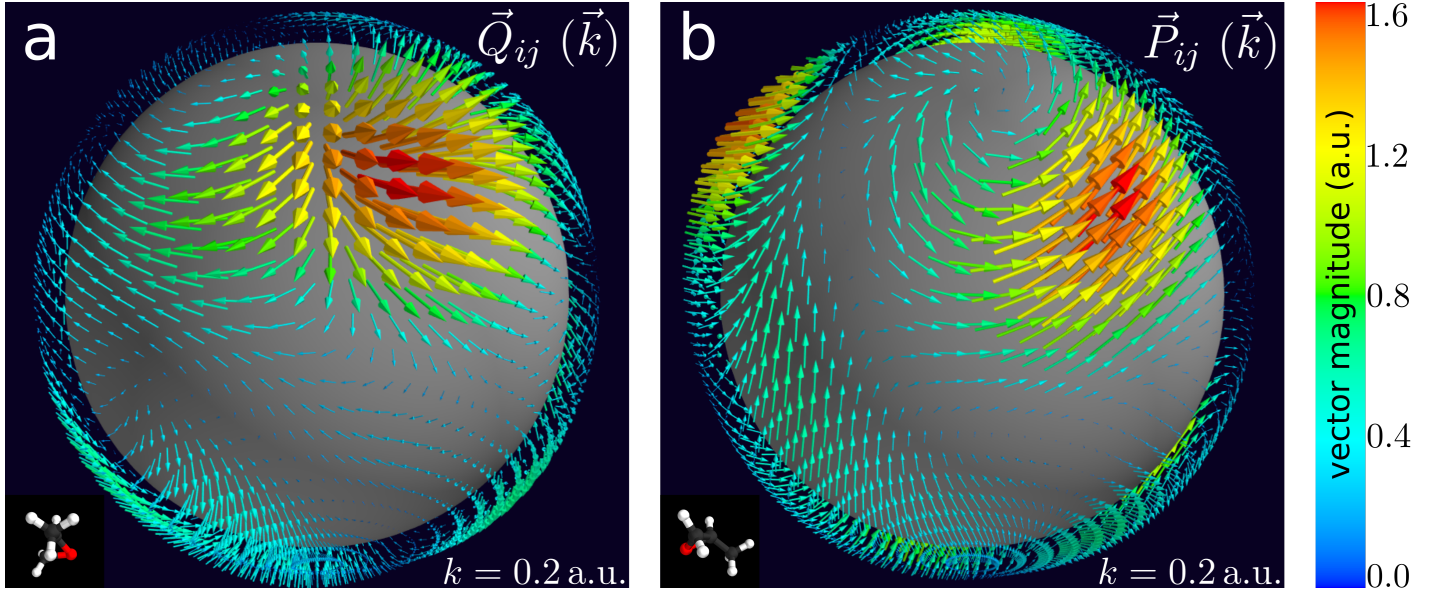


Figure 1 (a) Displacement $\vec{Q}_{ij}(\vec{k})$ [Eq. (8)] and (b) current $\vec{P}_{ij}(\vec{k})$ [Eq. (9)] quadratures of the geometric field $\vec{B}_{i,j}(\vec{k})$ [Eq. (7)] for $i=\text{LUMO}$ and $j=\text{LUMO}+1$ of the chiral molecule propylene oxide and photoelectron momentum $k = 0.2$ a.u. The molecular orientation is shown in the left bottom corner of each panel. Note that the quadratures are shown from different viewpoints.

to Eq. (1). For any number of states Eqs. (1,7) can be generalized as

$$\vec{B}(\vec{k}, t) = \frac{1}{2} \sum_{i,j} \left\{ i \left[\vec{d}_{kj} \times \vec{d}_{ki}^* \right] \right\} e^{i\phi_{ij}}. \quad (10)$$

We call $\vec{B}(\vec{k}, t)$ in Eq. (10) *geometric field in molecular photoionization*. Applying inversion ($\vec{r} \rightarrow -\vec{r}$, $\vec{k} \rightarrow -\vec{k}$) to reverse molecular handedness, we find that the displacement and current quadratures in left- (S) and right-handed (R) molecules are connected via $\vec{Q}_{ij}^{(S)}(\vec{k}) = \vec{Q}_{ij}^{(R)}(-\vec{k})$ and $\vec{P}_{ij}^{(S)}(\vec{k}) = \vec{P}_{ij}^{(R)}(-\vec{k})$. The geometric propensity field reflects the geometry of the molecular photoionization dipoles and gives rise to three classes of enantio-sensitive observables.

Three classes of anomalous enantio-sensitive observables

Enantio-sensitive photoionization observables are defined in the laboratory frame and originate from global invariants of the geometric propensity field – quantities surviving averaging over the directions of \vec{k} in the molecular frame. The **first** global invariant corresponds to non-zero *net* geometric field (integrated over all angles ϕ_k, θ_k characterizing the orientation of \vec{k} in the molecular frame, $d\Theta_k \equiv d\phi_k d\theta_k \sin \theta_k$):

$$\vec{B}_{ij}(k) \equiv \int \vec{B}_{ij}(\vec{k}) d\Theta_k \neq 0. \quad (11)$$

The **second** global invariant requires non-zero *net* radial component of the propensity field:

$$[\mathbf{B}_{\parallel}(k)]_{ij} \equiv \int \vec{B}_{ij}(\vec{k}) \cdot \hat{k} d\Theta_k \neq 0, \quad \hat{k} = \frac{\vec{k}}{k}. \quad (12)$$

The **third** global invariant includes an infinite array of multipoles ($l \geq 1$) of *net radial* and of the two *net tangential* components of the propensity field:

$$[\mathbf{B}_{\parallel}^{l,m}(k)]_{ij} \equiv \int \vec{B}_{ij}(\vec{k}) \cdot \hat{k} Y_{lm}(\theta_k, \phi_k) d\Theta_k \neq 0, \quad \hat{k} = \frac{\vec{k}}{k} \quad (13)$$

$$[\mathbf{B}_{\perp,1}^{l,m}(k)]_{ij} \equiv \int \vec{B}_{ij}(\vec{k}) \cdot \vec{\nabla}_k Y_{lm}(\theta_k, \phi_k) d\Theta_k \neq 0, \quad (14)$$

$$[\mathbf{B}_{\perp,2}^{l,m}(k)]_{ij} \equiv \int \vec{B}_{ij}(\vec{k}) \cdot [\hat{k} \times \vec{\nabla}_k] Y_{lm}(\theta_k, \phi_k) d\Theta_k \neq 0 \quad (15)$$

These quantities are the spherical multipole moments of the vector field $\vec{B}(\vec{k})$ (see e.g. [24]).

These three global invariants lead to three classes of enantio-sensitive observables in photoionization. We call these observables anomalous, in analogy to anomalous velocity in solids stemming from the Berry curvature. Their emergence or cancellation is determined by the time-reversal symmetry of the molecular bound states and the \vec{k} -inversion symmetries of the quadratures $\vec{Q}_{ij}(\vec{k}), \vec{P}_{ij}(\vec{k})$. It is convenient to introduce symmetric and anti-symmetric superpositions of the quadratures corresponding to left ($\vec{Q}_{ij}^{(S)}, \vec{P}_{ij}^{(S)}$) and right ($\vec{Q}_{ij}^{(R)}, \vec{P}_{ij}^{(R)}$) molecules:

$$\vec{Q}_{ij}^{\pm}(\vec{k}) = \frac{1}{2} [\vec{Q}_{ij}^{(S)}(\vec{k}) \pm \vec{Q}_{ij}^{(R)}(\vec{k})], \quad (16)$$

$$\vec{P}_{ij}^{\pm}(\vec{k}) = \frac{1}{2} [\vec{P}_{ij}^{(S)}(\vec{k}) \pm \vec{P}_{ij}^{(R)}(\vec{k})]. \quad (17)$$

The symmetric superpositions $\vec{Q}_{ij}^{+}(\vec{k}), \vec{P}_{ij}^{+}(\vec{k})$ are \vec{k} -even and the anti-symmetric superpositions $\vec{Q}_{ij}^{-}(\vec{k}), \vec{P}_{ij}^{-}(\vec{k})$ are \vec{k} -odd.

The **Class I** of enantio-sensitive observables relies on the existence of the net geometric field Eq. (11). Evidently, the k -odd quadratures $\vec{Q}_{ij}^{-}(\vec{k})$ and $\vec{P}_{ij}^{-}(\vec{k})$ do not contribute to this integral. We show (see Appendix A) that Eq. (11) cannot be satisfied when ionization takes place from a real (time-even) state. Thus, $\vec{Q}_{ij}^{+}(\vec{k})$ also does not contribute to the net geometric field, which only arises due to the symmetric quadrature $\vec{P}_{ij}^{+}(k)$:

$$\vec{B}_{ij}(k) = \int \vec{B}_{ij}(\vec{k}) d\Theta_k = \int \vec{P}_{ij}^{+}(\vec{k}) d\Theta_k \sin \phi_{ij} \equiv \vec{P}_{ij}^{+}(k) \sin \phi_{ij} \quad (18)$$

Thus, the new enantio-sensitive observables of Class I can only appear if photoionization by a circularly polarized field occurs from current-carrying states ($\sin \phi_{ij} \neq 0$). For example, such states can be generated by a pump pulse with ionization following ultrafast excitation of a coherent superposition of eigenstates. The fact that the net field $\vec{B}(k)$ emerges only in systems undergoing dynamics makes it an important player in attosecond photochemistry. In contrast to ring currents excited in atoms or non-chiral molecules by circularly polarized fields [25–27], chiral molecules present an example of a system where excited currents do not vanish in the molecular frame upon averaging over random molecular orientations, because they are protected by the rotationally invariant geometric property of *molecular handedness*. The net geometric field in the molecular frame (18) leads to enantio-sensitive molecular orientation by ionization (see below) and is an example of charge directed reactivity emerging solely due to molecular handedness.

The **Class II** of enantio-sensitive observables relies on the existence of the *net radial* component of the geometric field Eq. (12). Clearly, the symmetric quadratures $\vec{Q}^+(\vec{k})$ and $\vec{P}^+(\vec{k})$ do not contribute to $B_{\parallel}(k)$, leaving us with the following global invariants allowed by symmetries:

$$[B_{\parallel}(k)]_{ij} = [Q_{\parallel}^-(k)]_{ij} \cos \phi_{ij} + [P_{\parallel}^-(k)]_{ij} \sin \phi_{ij}, \quad (19)$$

$$[Q_{\parallel}^-(k)]_{ij} = \int \vec{Q}_{ij}^-(\vec{k}) \cdot \hat{k} d\Theta_k \quad \hat{k} = \frac{\vec{k}}{k}, \quad (20)$$

$$[P_{\parallel}^-(k)]_{ij} = \int \vec{P}_{ij}^-(\vec{k}) \cdot \hat{k} d\Theta_k, \quad \hat{k} = \frac{\vec{k}}{k}. \quad (21)$$

The *net radial* component $B_{\parallel}(k)$ is proportional to the flux of the field $\vec{B}(\vec{k})$, which is responsible for the PECD[19] [see Eq. (4)]. Thus, the global invariant $[Q_{\parallel}^-(k)]_{ij}$ for $i = j$ leads to PECD for photoionization from a real stationary state. PECD from the superposition of states (time-dependent PECD[28]) also involves the complementary quadrature $[P_{\parallel}^-(k)]_{ij}$.

The **Class III** of enantio-sensitive observables originates from an infinite array of multipoles ($l \geq 1$) of *net radial* and of the two *net tangential* components of the propensity field: Eqs. (13,14,15). The parity of spherical harmonics $Y_{lm}(\vec{k}) = (-1)^l Y_{lm}(-\vec{k})$ dictates that even multipoles $[B_{\parallel}^{l=2n,m}(k)]_{ij}$ and $[B_{\perp,1}^{l=2n,m}(k)]_{ij}$ can only emerge due to the asymmetric quadratures $\vec{Q}_{ij}^-(\vec{k})$ and $\vec{P}_{ij}^-(\vec{k})$, while the odd multipoles $[B_{\parallel}^{l=2n+1,m}(k)]_{ij}$ and $[B_{\perp,1}^{l=2n+1,m}(k)]_{ij}$ can emerge only due to the symmetric quadratures $\vec{Q}_{ij}^+(\vec{k})$ and $\vec{P}_{ij}^+(\vec{k})$. For the $[B_{\perp,2}^{l,m}(k)]_{ij}$ multipoles it is the other way around: the terms with even l may only appear due to the symmetric quadratures $\vec{Q}_{ij}^+(\vec{k})$ and $\vec{P}_{ij}^+(\vec{k})$, while the terms with odd l may

emerge only due to $\vec{Q}_{ij}^-(\vec{k})$ and $\vec{P}_{ij}^-(\vec{k})$.

Class III observables emerge in two- or multi-photon ionization. For example, quadrupolar [$l = 1$ in Eq. (13)] PECD currents [29] emerge in photoionization of chiral molecules triggered by orthogonally polarized two-color $\omega - 2\omega$ fields [30–32]. Other members of this class have not been identified so far.

New anomalous enantio-sensitive observables

While the Class II and some of the Class III observables have already been detected in experiments, the Class I of anomalous enantio-sensitive observables have not been explored yet. This class requires excitation of current prior to photoionization. Consider a pump-probe set-up with two pulses copropagating along the \hat{z} axis of the laboratory frame. The linearly polarized pump pulse excites a coherent superposition of two states with energy difference ω_{12} in a randomly oriented molecular ensemble. The excitation is probed via photoionization by a circularly polarized probe. The net geometric field is: $\vec{B}_{12}(k, t) = \vec{P}_{12}^+(k) \sin(\omega_{12}t)$. Suppose that \hat{e}_B^M is a unit polar molecular frame vector (superscript M) collinear with the net geometric field $\hat{e}_B^M \parallel \vec{P}_{12}(k)$ in the molecular frame of a given enantiomer. The scalar product $\hat{e}_B^M \cdot \vec{P}_{12}(k) = v|\vec{P}_{12}(k)|$ is a pseudoscalar, which has opposite signs ($v = \pm 1$) in opposite enantiomers. Upon photoionization the same vector \hat{e}_B^L in the laboratory frame (superscript L) is:

$$\langle \hat{e}_B^L(k, \tau) \rangle = R \langle \hat{e}_B^L(k, \tau) \rangle_{\text{isotropic}}, \quad (22)$$

$$\langle \hat{e}_B^L(k, \tau) \rangle_{\text{isotropic}} = \frac{1}{9} C \sigma v (\vec{d}_{10} \cdot \vec{d}_{20}) \left| \vec{P}_{12}^+(k) \right| \sin(\omega_{12} \tau) \hat{z}, \quad (23)$$

where R accounts for the molecular alignment induced by the pump,

$$R \equiv \frac{6}{5} \left[1 - \frac{1}{2} \frac{(\vec{d}_{10} \cdot \hat{e}_B^M)(\vec{d}_{20} \cdot \hat{e}_B^M)}{(\vec{d}_{10} \cdot \vec{d}_{20})} \right], \quad (24)$$

while $\langle \hat{e}_B^L(k, \tau) \rangle_{\text{isotropic}}$ ignores it; \vec{d}_{10} and \vec{d}_{20} are the molecular frame excitation dipoles and C encodes the pump and probe Fourier components at the excitation and photoionization frequencies correspondingly[33] (see Appendix B and Appendix C):

$$C \equiv |\mathcal{E}_1^*(\omega_{20}) \mathcal{E}_2^*(\omega_{k2}) \mathcal{E}_1(\omega_{10}) \mathcal{E}_2(\omega_{k1})|. \quad (25)$$

Eqs. (22, 23) show that the oscillating net geometric field $\left| \vec{P}_{12}^+(k) \right| \sin(\omega_{12} \tau)$ dictates the orientation of the molecular frame vector $\hat{e}_B^M(k) \parallel \vec{P}_{12}^+(k)$ along the \hat{z} -axis perpendicular to the polarization of the

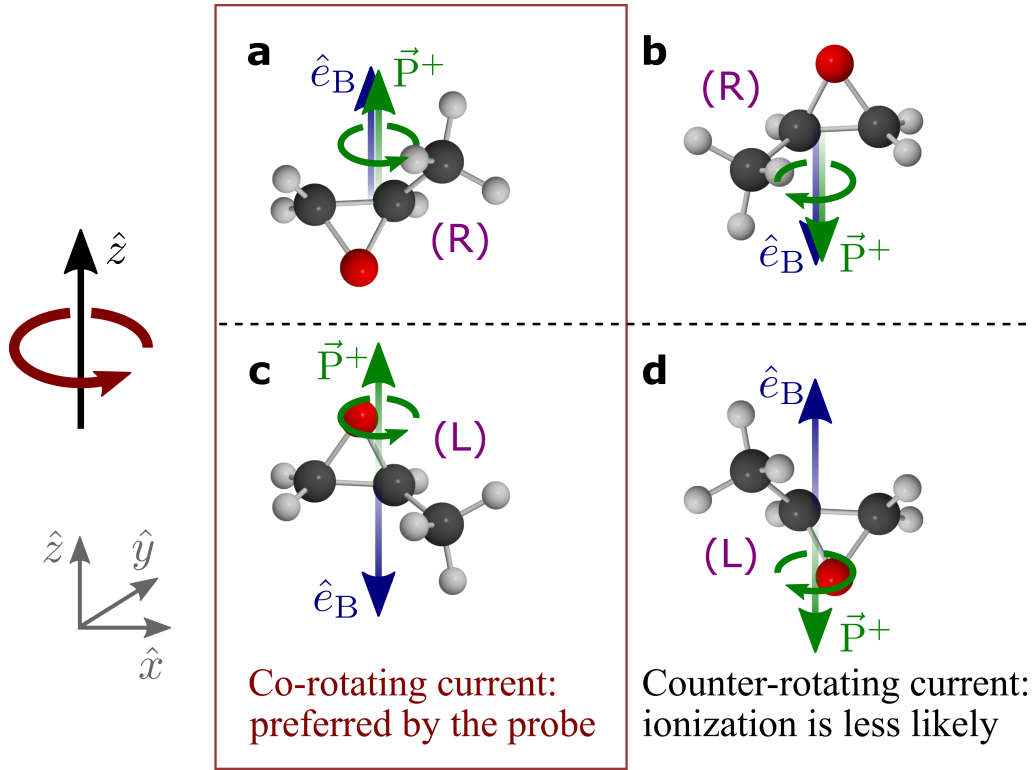


Figure 2 Relative orientations of the molecular vectors \vec{e}_B and \vec{P}^+ for opposite molecular orientations and opposite enantiomers in propylene oxide for $k = 0.2$ a.u. and a superposition of LUMO and LUMO+1. The red circular arrow shows the rotation direction of the circularly polarized field. The green circular arrows show the circular current in the excited states right before ionization takes place. Photoionization rates are higher for orientations (a) and (c) than for (b) and (d) because ionization is more effective when the electronic current (circular green arrow fixed to \vec{P}^+) and the electric field rotate in the same direction. This difference in photoionization rates causes enantio-sensitive orientation.

circularly polarized probe. The direction of the vector $\hat{e}_B^L(k, \tau)$ is opposite in opposite enantiomers, because $\vec{P}_{12}^+(k) \cdot \hat{e}_B^M = v |\vec{P}_{12}^+(k)|$ is a molecular pseudoscalar that has opposite sign ($v = \pm 1$) in opposite enantiomers. The orientation is also reversed when the direction of rotation ($\sigma = \pm 1$) of the circularly polarized probe pulse is reversed.

Eqs. (22, 23) predict that the enantio-sensitive orientation (the molecular orientation circular dichroism, MOCD) oscillates as a function of the pump-probe delay, reaching maximal positive or negative values for $\tau = (2n - 1)\pi/(2\omega_{12})$, n is a positive integer. Photoionization at opportune times using a circularly polarized probe induces enantio-sensitive orientation of both the molecular cations and of the excited neutrals that were not ionised, with the orientation of the neutrals opposite to that of the cations.

Figure 2 shows the direction of the molecular orientation \hat{e}_B^L arising when the excitation of LUMO and LUMO+1 in propylene oxide is followed by photoionization into the states with momentum $k =$

0.2 a.u., for the left- and right-handed enantiomers. The quadrature $\vec{P}_{12}^+(k)$, where $|2\rangle = |LUMO + 1\rangle$, $|1\rangle = |LUMO\rangle$, has the same direction in the left- and right-handed enantiomers, but the pseudoscalar v has opposite signs for the opposite enantiomers, corresponding to opposite orientations of left and right molecular ions with respect to the laboratory \hat{z} axis. To calculate the geometric field, we have used the photo-excitation and photoionization dipoles computed using the DFT-based approach developed in [34]. This approach yields excellent agreement with the experimental data for one-photon ionization of chiral molecules [35–39].

Figure 3 compares the quadratures responsible for Class I and Class II enantio-sensitive observables for the same excitation. The magnitude of the net quadrature $|\vec{P}_{12}^+(k)|$ quantifying the MOCD is substantially larger than each of the quadratures $\left[Q_{\parallel}^{-M}(k)\right]_{12}$ and $\left[P_{\parallel}^{-M}(k)\right]_{12}$ quantifying the time-dependent PECD (TD-PECD):

$$\vec{j}_{\text{TD-PECD}}(k, \tau) = \frac{1}{9} C \sigma k (\vec{d}_{10}^M \cdot \vec{d}_{20}^M) \left\{ \cos(\omega_{12} \tau) \left[Q_{\parallel}^{-M}(k)\right]_{12} + \sin(\omega_{12} \tau) \left[P_{\parallel}^{-M}(k)\right]_{12} \right\} \hat{z}. \quad (26)$$

In Eq. (26) we have ignored the molecular alignment by the pump and omitted the time-independent contributions to facilitate the comparison with Eq. (23) for MOCD.

Figure 3 shows that the enantio-sensitive orientation is at least of the same order of magnitude as the enantio-sensitive signal in TD-PECD [28]. Importantly, TD-PECD and MOCD involve completely different components of the geometric propensity field and therefore expose different and complementary aspects of chiral dynamics in molecules.

Qualitatively, the orientation induced by photoionization can be understood as follows. First, a linearly polarized pump excites a couple of excited states $|1\rangle$ and $|2\rangle$ and produces a current \vec{j}_{12} oscillating at frequency ω_{12} . Suppose that this current goes from the ‘head’ of a molecule to its ‘tail’ in the molecular frame. For two molecules oppositely oriented in the laboratory frame (see Figs. 2a and 2b), \vec{j}_{12} will have the same direction in the molecular frame [40]. Second, like a helix, the chiral structure of the molecule converts this linear current into a circular current, which will have the same direction of rotation in the molecular frame for both orientations. Thus, in the laboratory frame, the two oppositely oriented molecules will display circular currents rotating in opposite directions (see circular arrows in Figs. 2a and 2b). Due to the propensity rules in one-photon ionization, explicitly quantified by the geometric propensity field $\vec{B}_{12}(\vec{k})$, the circularly polarized probe pulse ‘selects’ (or preferentially ionizes) the orientation with the current co-rotating with the probe pulse. This leads to a difference in the photoionization yields resulting from each orientation and thus to the emergence of oriented molecular ions. Note that for the opposite enantiomer, the chiral structure of the molecules

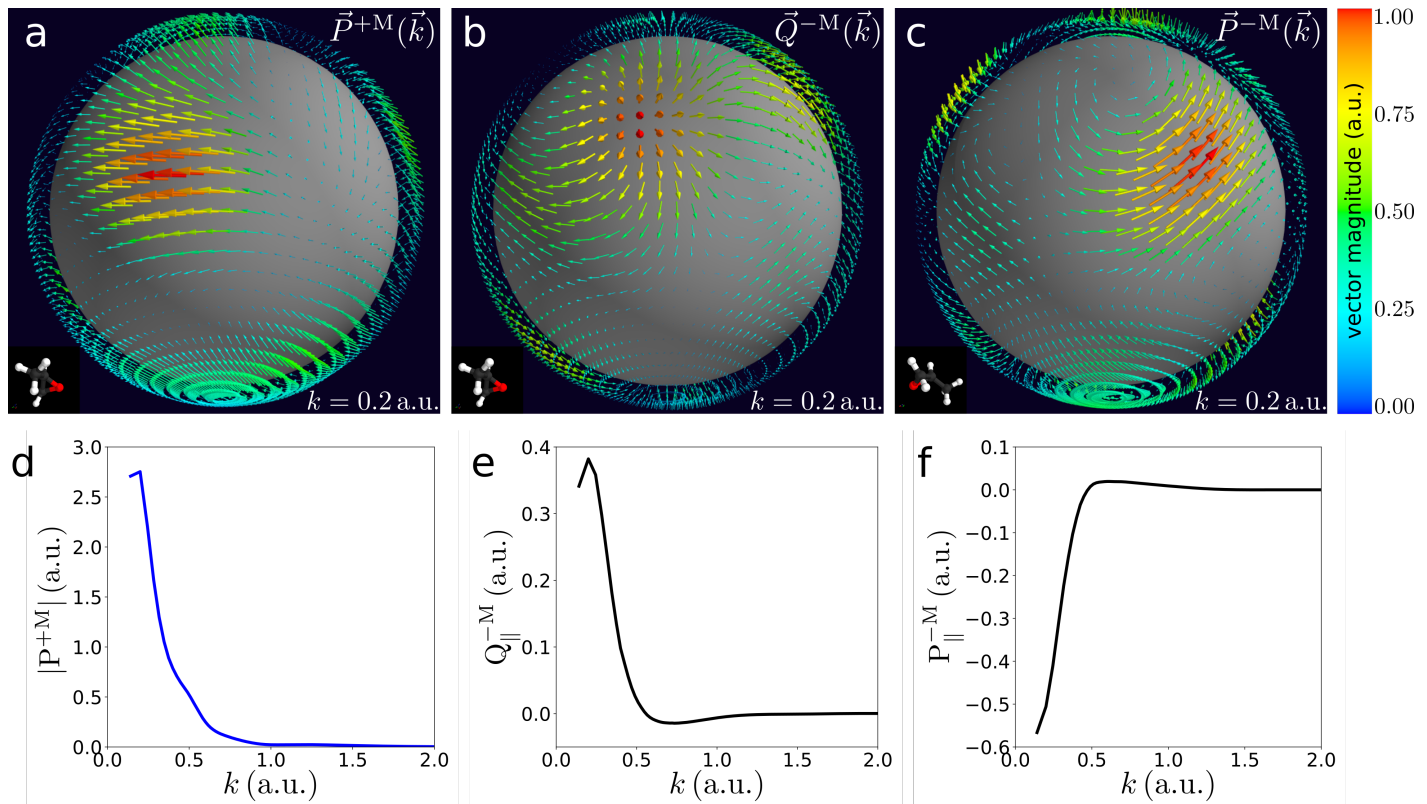


Figure 3 Propensity field and its global invariants emerging upon excitation of LUMO and LUMO+1 orbitals in propylene oxide. (a) The symmetric quadrature $\vec{P}^{+M}(\vec{k})$ [Eq. (17)] for $k = 0.2$ a.u. and (d) the magnitude of its net value $|\vec{P}^{+M}(k)|$ [Eq. (18)], which governs Class I observables, such as enantio-sensitive molecular orientation (MOCD) [Eqs. (22, 23)]. (b) Asymmetric quadratures $\vec{Q}^{-M}(\vec{k})$ [Eq. (16)] and (c) $\vec{P}^{-M}(\vec{k})$ [Eq. 17] for $k = 0.2$ a.u. and (e) the net values of their radial components $Q_{||}^{-M}(k)$ [Eq. (20)] and (f) $P_{||}^{-M}(k)$ [Eq. (21)], which govern Class II observables, such as the TD-PECD [Eq. (26)].

creates the opposite circulating current in the molecular frame, and thus the probe-pulse ‘selects’ the opposite orientation (see Figs. 2c and 2d).

Importantly, the difference in the angle-integrated ionization yields for the two opposite orientations is proportional to the projection of the net propensity field $\vec{B}_{12}(k)$ on the laboratory \hat{z} axis. Thus, the propensity rule ‘selecting’ molecular orientations with co-rotating current is most pronounced for orientations where $\vec{B}_{12}(k) \parallel \hat{z}$, which explains why $\vec{B}_{12}(k)$ is the molecular axis becoming maximally oriented. The fact that the photoionization yield depends on the direction of the current excited in the chiral molecule prior to photoionization not only explains the emergence MOCD but is also an example of enantio-sensitive charge directed reactivity.

Figure 4 shows the degree of orientation of the molecular ions due to subsequent ionisation by the probe pulse calculated using the DFT-based matrix elements, dipole couplings and Eq. (22). The strength of the effect is characterized by the fraction of oriented ions normalized to total ionization

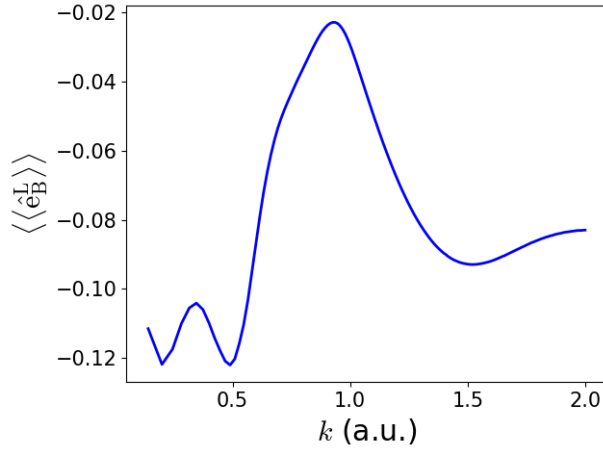


Figure 4 Degree of orientation [Eq. (43)] corresponding to excitation of LUMO and LUMO+1 in propylene oxide and subsequent ionization by circularly polarized field for $\omega_{12}\tau = \pi/2$, $\nu=1$, $\sigma = 1$.

yield (averaged over pump-probe delay), see Appendix C. Having $\langle\cos\Theta\rangle = -0.12$ for $k = 0.2$ a.u. means that roughly 59 out of 100 molecules have $\hat{e}_B \cdot \hat{z} < 0$ and 41 out of 100 molecules have $\hat{e}_B \cdot \hat{z} > 0$ (see Appendix C). Thus, a very significant degree of enantio-sensitive orientation results from the excitation of chiral dynamics in valence shells.

Outlook

Geometric magnetism underlies efficient enantio-sensitive observables in molecular photoionization. We see several future directions associated with the phenomenon of geometric magnetism in photoionization of chiral molecules.

Valence-shell MOCD can be induced by exciting electronic or vibronic degrees of freedom and thus can be achieved with pulses of various durations: from sub-femtoseconds to picoseconds. An interesting future direction is to use enantio-sensitive molecular orientation (MOCD) which occurs in neutral molecules and molecular ions for (i) quantification of helical currents in chiral molecules, (ii) enantio-separation and (iii) ultrafast molecular imaging with oriented chiral molecules.

MOCD can also be induced by core excitations with short, few-femtosecond, X-ray pulses. Localised site-specific core excitations could allow one to initiate currents from different locations inside the molecule and probe the orientation of the most efficient “molecular cork-screw”. Probing the induced electronic excitations should likely be done before the core-hole decay due to e.g. the Auger process. Molecular fragmentation, which may be induced by such decay, could be beneficial for detecting MOCD via angular distributions of fragments.

We have found that MOCD can also be induced using circularly polarized pump pulse and linearly polarized probe. In this case, MOCD emerges due to the helical PXCD current [41] excited in bound

states [42] and does not involve the geometry of photoionization dipoles. MOCD induced by circularly polarized pump and probe pulses records the interference between the PXCD mechanism of MOCD[42] and the anomalous geometric mechanism described here. Such interference presents a new opportunity to characterize the geometric field experimentally.

Another interesting direction is the identification of new members of Classes I, II, and III of enantio-sensitive observables predicted in this work.

The geometric field in chiral molecules, described here, is a newly recognised member of the family of geometric fields. It may allow one to explore the link between chiral and topological phenomena, and possibly induce new topology-driven phenomena such as quantized circular dichroism in photoionization of chiral molecules.

Acknowledgments

We gratefully acknowledge many enlightening discussions with Prof. Misha Ivanov. We thank Dr. Rui Emanuel Ferreira da Silva and Dr. Álvaro Jiménez Galán for their comments on the manuscript and Dr. Emilio Pisanty for suggesting the acronym "MOCD". OS is grateful to Ms. Julia Riedel for applying right pressure at right times. O.S., D.A., A.F.O. acknowledge funding from Deutsche Forschungsgemeinschaft (SM 292/5-2). A.F.O. acknowledges grants supporting research at ICFO: Agencia Estatal de Investigación ("Severo Ochoa" Center of Excellence CEX2019-000910-S, National Plan FIDEUA PID2019-106901GB-I00/10.13039 / 501100011033, FPI), Fundació Privada Cellex, Fundació Mir-Puig, Generalitat de Catalunya (AGAUR Grant No. 2017 SGR 1341, CERCA program) and EU Horizon 2020 Marie Skłodowska-Curie grant agreement No 101029393, supporting his research on chirality. D.A. acknowledges funding from the Royal Society (URF/R1/201333) supporting his research on chirality.

Appendix A

Operator approach and time-reversal symmetry of the net geometric field

Here we prove that

$$\int d\Theta_k \vec{Q}_{ij}(\vec{k}) = 0 \quad (27)$$

when $|\psi_i\rangle$ and $|\psi_j\rangle$ are time-even states, which we use in Eq. (18).

The time-reversal symmetry plays a central role in enabling the net geometric field. To consider the parity of the geometric field (or its quadratures) with respect to time-reversal, it is convenient[43] to

introduce an operator approach. Eq. (7) of the main text can be rewritten in the following form:

$$\vec{B}_{ij}(\vec{k}, \phi_{ij}) = -\frac{1}{2}i \left[\vec{d}_{ki}^* \times \vec{d}_{kj} \right] e^{i\phi_{ij}} + \text{c.c.} = -\frac{1}{2}\vec{F}_{ij}e^{i\phi_{ij}} + \text{c.c.}, \quad (28)$$

where $\vec{F}_{ij}(\vec{k}) \equiv i \left[\vec{d}_{ki}^* \times \vec{d}_{kj} \right]$ and thus,

$$\vec{Q}_{ij}(\vec{k}) \equiv -\Re \left\{ \vec{F}_{ij}(\vec{k}) \right\}, \quad (29)$$

$$\vec{P}_{ij}(\vec{k}) \equiv \Im \left\{ \vec{F}_{ij}(\vec{k}) \right\}. \quad (30)$$

To establish the parity of net quadratures with respect to time-reversal, it is sufficient to consider the time-reversal parity of the net $\vec{F}_{ij}(\vec{k})$:

$$\vec{F}_{ij} \equiv \int d\Theta_k i \vec{d}_{k,i}^* \times \vec{d}_{k,j}. \quad (31)$$

Analogously to the procedure in Ref. [43], we rewrite \vec{F}_{ij} as the matrix element of an operator $\hat{\vec{F}}$:

$$\vec{F}_{ij} \equiv \int d\Theta_k i \vec{d}_{k,i}^* \times \vec{d}_{k,j} = \int d\Theta_k i \langle \psi_i | \hat{\vec{r}} | \psi_k^{(-)} \rangle \times \langle \psi_k^{(-)} | \hat{\vec{r}} | \psi_j \rangle = \langle \psi_i | \hat{\vec{F}} | \psi_j \rangle, \quad (32)$$

where the operator $\hat{\vec{F}}$ in vector and component form is given by

$$\hat{\vec{F}} \equiv i \int d\Theta_k \hat{\vec{r}} | \psi_k^{(-)} \rangle \langle \psi_k^{(-)} | \hat{\vec{r}}, \quad \hat{F}_a = i \epsilon_{abc} \int d\Theta_k \hat{r}_b \hat{P}_k \hat{r}_c = i \epsilon_{abc} \hat{r}_b \hat{P}_k \hat{r}_c, \quad (33)$$

and $\hat{P}_k \equiv \int d\Theta_k | \psi_k^{(-)} \rangle \langle \psi_k^{(-)} |$ is the projector on the subspace of all states with energy $E = k^2/2$. Since $\hat{\vec{r}}$ and \hat{P}_k are Hermitian, $\hat{\vec{F}}$ is also Hermitian:

$$\hat{F}_a^\dagger = (i \epsilon_{abc} \hat{r}_b \hat{P}_k \hat{r}_c)^\dagger = -i \epsilon_{abc} \hat{r}_c \hat{P}_k \hat{r}_b = i \epsilon_{acb} \hat{r}_c \hat{P}_k \hat{r}_b = \hat{F}_a. \quad (34)$$

Now we want to see how time reversal considerations constraint the matrix elements of $\hat{\vec{F}}$. Let \hat{T} be the time-reversal operator (see e.g. sec. 4.4 in Ref. [44]). \hat{T} converts a state $|\alpha\rangle$ into its time-reversed counterpart $|\tilde{\alpha}\rangle = \hat{T}|\alpha\rangle$, which we denote by a tilde. \hat{T} is anti-unitary, i.e. $\langle \tilde{\alpha} | \tilde{\beta} \rangle = \langle \alpha | \beta \rangle^*$ and $T(c_1|\alpha\rangle + c_2|\beta\rangle) = c_1^*|\tilde{\alpha}\rangle + c_2^*|\tilde{\beta}\rangle$. A Hermitian operator \hat{A} is time-even (+) or time-odd (−) when $\hat{T}\hat{A} = \pm\hat{A}\hat{T}$. Time parity restricts the matrix elements of \hat{A} according to $\langle \alpha | \hat{A} | \beta \rangle = \pm \langle \tilde{\alpha} | \hat{A} | \tilde{\beta} \rangle^*$. In particular, if \hat{A} is time-odd and the states are time-even (i.e. $|\tilde{\alpha}\rangle = |\alpha\rangle$ and $|\tilde{\beta}\rangle = |\beta\rangle$), it follows that

$\langle \alpha | \hat{A} | \beta \rangle = -\langle \alpha | \hat{A} | \beta \rangle^*$ and thus $\Re\{\langle \alpha | \hat{A} | \beta \rangle\} = 0$.

For \hat{P}_k we have

$$\hat{T} \hat{P}_k |\phi\rangle = \hat{T} \left[\int d\Theta_k |\psi_k^{(-)}\rangle \langle \psi_k^{(-)}| \phi \rangle \right] = \int d\Theta_k |\tilde{\psi}_k^{(-)}\rangle \langle \psi_k^{(-)}| \phi \rangle^* = \int d\Theta_k |\tilde{\psi}_k^{(-)}\rangle \langle \tilde{\psi}_k^{(-)}| \tilde{\phi} \rangle = \hat{\tilde{P}}_k \hat{T} |\phi\rangle \quad (35)$$

where $\hat{\tilde{P}}_k \equiv \int d\Theta_k |\tilde{\psi}_k^{(-)}\rangle \langle \tilde{\psi}_k^{(-)}|$ also projects on the subspace of all states with energy $E = k^2/2$. Since \hat{P}_k and $\hat{\tilde{P}}_k$ project on the same subspace we must have $\hat{P}_k = \hat{\tilde{P}}_k$ and thus \hat{P}_k is time-even. Furthermore, since $\hat{\tilde{r}}$ is also time-even, we can use the anti-unitary character of \hat{T} to find that

$$\hat{T} \hat{F}_a |\phi\rangle = \hat{T} (i\epsilon_{abc} \hat{r}_b \hat{P}_k \hat{r}_c |\phi\rangle) = -i\epsilon_{abc} \hat{r}_b \hat{P}_k \hat{r}_c \hat{T} |\phi\rangle = -\hat{F}_a \hat{T} |\phi\rangle, \quad (36)$$

which means that $\hat{\tilde{F}}$ is time-odd. Thus, $\Re\{\vec{F}_{ij}\} = 0$ when $|\psi_i\rangle$ and $|\psi_j\rangle$ are time-even states. Finally, using Eqs. (29,30) we obtain for time-even states $|\psi_i\rangle$ and $|\psi_j\rangle$:

$$\int d\Theta_k \vec{Q}_{ij}(\vec{k}) = - \int d\Theta_k \Re\{\vec{F}_{ij}(\vec{k})\} = -\Re\{\vec{F}_{ij}\} = 0, \quad (37)$$

Further, the time-odd parity of $\hat{\tilde{F}}$ does not restricts the value of net momentum quadrature, which in general is non-zero:

$$\int d\Theta_k \vec{P}_{ij}(\vec{k}) = \int d\Theta_k \Im\{\vec{F}_{ij}(\vec{k})\} = \Im\{\vec{F}_{ij}\} \neq 0. \quad (38)$$

Appendix B

The origin of Class I enantio-sensitive observables

The connection between enantio-sensitive observables in photoionization and the geometric propensity field becomes evident as soon as we consider the photoionization yield $W(k)$ into energy $E = k^2/2$ for a fixed in space molecule ionised by circularly polarized light in the electric dipole approximation [45]:

$$W(k, \rho) \propto \int d\Theta_k |a_{\vec{k}c}|^2 \quad (39)$$

$$|a_{\vec{k}c}|^2 = \frac{1}{2} |\mathcal{E}(\omega)|^2 \left\{ |\vec{d}_{\vec{k}c}^{\text{L}}(\rho) \cdot \hat{x}|^2 + |\vec{d}_{\vec{k}c}^{\text{L}}(\rho) \cdot \hat{y}|^2 + \sigma \vec{B}^{\text{L}}(\vec{k}, \rho) \cdot \hat{z} \right\}. \quad (40)$$

Here $a_{\vec{k}c}$ is the amplitude of ionization from a complex-valued randomly oriented bound state $|\psi_c\rangle$ (at this point we do not specify how this state was created in a randomly oriented molecular ensemble and assume that it is given to us) into the final state with photoelectron momentum \vec{k} , $\mathcal{E}(\omega)$ is the Fourier component of the light field at the transition frequency ω [46], $\sigma = \pm 1$ for light rotating

clockwise/counterclockwise in the xy plane, integration over $d\Theta_k$ describes averaging over the directions of the photoelectron momentum, ρ denotes the Euler angles characterizing the orientation of the molecular frame relative to the laboratory frame, the vectors \hat{x} , \hat{y} , and \hat{z} denote the axes of the laboratory frame, $\vec{d}_{kc}^L(\rho)$ is the photoionization dipole in the laboratory frame (denoted by superscript L), and $\vec{B}^L(\vec{k}, \rho)$ is the propensity field in the laboratory frame.

Using Eq. (40) we formally obtain the expression for the orientation-averaged value of an arbitrary vectorial observable $\vec{V}^L(k)$ of the molecular cation:

$$\begin{aligned}\langle \vec{V}^L(k) \rangle &\equiv \int d\rho W(k, \rho) \vec{V}^L(\rho) \\ &= \frac{1}{2} |\mathcal{E}(\omega)|^2 \sigma \int d\rho \left[\int \vec{B}^L(\vec{k}, \rho) \cdot \hat{z} d\Theta_k \right] \vec{V}^L \\ &= \frac{1}{6} |\mathcal{E}(\omega)|^2 \sigma \left(\vec{B}^M(k) \cdot \vec{V}^M \right) \hat{z}.\end{aligned}\tag{41}$$

Here the superscripts L and M indicate that the respective vectors are expressed with respect to the laboratory frame or the molecular frame correspondingly. Equation (41) shows that after ionization with circularly polarized light, the ensemble-averaged value of the vector V (fixed in the molecular frame), will have an *anomalous* (proportional to the geometric field) enantio-sensitive component along the direction perpendicular to the polarization plane.

Appendix C

Equations describing the MOCD

Suppose that \hat{e}_B^M is a unit polar vector collinear with the net propensity field $\hat{e}_B^M \parallel \vec{B}^M(k)$ in the molecular frame of a given enantiomer. The scalar product $\hat{e}_B^M \cdot \vec{B}^M(k) = v |\vec{B}^M(k)|$ is a pseudoscalar ($v = \pm 1$), which has opposite signs in opposite enantiomers. The orientation of the vector \hat{e}_B^M in the laboratory frame \hat{e}_B^L is given by [see Eq. (41)]:

$$\langle \hat{e}_B^L(k) \rangle = \frac{1}{6} |\mathcal{E}(\omega)|^2 \sigma v |\vec{B}^M(k)| \hat{z}.\tag{42}$$

Therefore, Eqs. (41) and (42) predict enantio-sensitive orientation of molecular ions by ionization. The molecular-frame vector $\hat{e}_B^M(k) \parallel \vec{B}^M(k)$ gets oriented along the laboratory \hat{z} -axis (perpendicular to the polarization of the circularly polarized probe).

Now we can specify the procedure of exciting the state $|\psi_c\rangle$ in randomly oriented molecular ensemble. The complex-valued state $|\psi_c\rangle$ corresponds to excitation of complex superposition of states

prior to photoionization, which can be excited with a linearly polarized pump pulse.

Using our approach [45, 47] we can calculate the orientation of the vector \hat{e}_B^\perp in a molecular cation analytically for the excitation of two intermediate states with energy difference $\omega_{2,1}$ in an ensemble of randomly oriented chiral molecules. Eqs. (22,23) of the main text can be obtained using Eqs. (30)-(35) in Ref.[45] and replacing \vec{k} by \hat{e}_B , choosing a pump linearly polarized along either \hat{x} , or \hat{y} , and a probe circularly polarized in the xy plane (both pulses are transform limited). To express all resulting terms via the vector product of two ionization dipoles, we used the Binet-Cauchy identity $(\vec{A} \times \vec{B}) \cdot (\vec{C} \times \vec{D}) = (\vec{A} \cdot \vec{C})(\vec{B} \cdot \vec{D}) - (\vec{A} \cdot \vec{D})(\vec{B} \cdot \vec{C})$ and the vector triple product identity $\vec{A} \times (\vec{B} \times \vec{C}) = (\vec{A} \cdot \vec{C})\vec{B} - (\vec{A} \cdot \vec{B})\vec{C}$.

Eq. (26) of the main text can be obtained using Eqs. (30)-(35) in Ref.[45], choosing a pump linearly polarized along either \hat{x} , or \hat{y} , and a probe circularly polarized in the xy plane (both pulses are transform limited).

The strength of the effect is characterized by the fraction of oriented ions normalized to total ionization yield (averaged over pump-probe delay).

$$\langle \langle \hat{e}_B^\perp(k, \tau) \rangle \rangle \equiv \frac{\int d\rho \hat{e}_B^\perp(\rho) W(k, \rho)}{\int d\rho \bar{W}(k, \rho)}, \quad (43)$$

$$\int d\rho \bar{W}(k, \rho) = \sum_{i=1,2} \frac{|C_i|^2}{30} \int d\Theta_k \left[3 \left| \vec{d}_{i0}^M \right|^2 \left| \vec{d}_{ki}^M \right|^2 - \left| \vec{d}_{i0}^M \cdot \vec{d}_{ki}^M \right|^2 \right], \quad (44)$$

and $C_i \equiv -\mathcal{C}(\omega_{i0})\mathcal{C}(\omega_{ki})$.

An estimate of the number of ‘up’ N_+ and ‘down’ N_- molecules for $\langle \cos \Theta \rangle = -0.12$ can be performed using a simple model for the angular distribution of oriented molecules: $\Psi(\Theta) = a_0 Y_{00}(\Theta) + a_1 Y_{10}(\Theta)$, where $a_0^2 + a_1^2 = 1$. Then $\langle \cos \Theta \rangle = \int_0^\pi d\Theta \int_0^{2\pi} d\Phi \sin \Theta \cos \Theta |\Psi(\Theta)|^2$, and we can obtain $N_+ \equiv \int_0^{\pi/2} d\Theta \int_0^{2\pi} d\Phi \sin \Theta |\Psi(\Theta)|^2 = \frac{1}{4}(2 + 3\langle \cos \Theta \rangle) = 0.41$ and $N_- \equiv \int_{\pi/2}^\pi d\Theta \int_0^{2\pi} d\Phi \sin \Theta |\Psi(\Theta)|^2 = 1 - N_+ = 0.59$.

-
- [1] M. V. Berry, Quantal phase factors accompanying adiabatic changes, Proceedings of the Royal Society of London. A. Mathematical and Physical Sciences **392**, 45 (1984).
 - [2] D. Xiao, M.-C. Chang, and Q. Niu, Berry phase effects on electronic properties, Rev. Mod. Phys. **82**, 1959 (2010).
 - [3] B. Ritchie, Theory of the angular distribution of photoelectrons ejected from optically active molecules

- and molecular negative ions, *Phys. Rev. A* **13**, 1411 (1976).
- [4] I. Powis, Photoelectron circular dichroism of the randomly oriented chiral molecules glyceraldehyde and lactic acid, *The Journal of Chemical Physics* **112**, 301 (2000).
 - [5] N. Böwering, T. Lischke, B. Schmidtke, N. Müller, T. Khalil, and U. Heinzmann, Asymmetry in photoelectron emission from chiral molecules induced by circularly polarized light, *Phys. Rev. Lett.* **86**, 1187 (2001).
 - [6] L. Nahon, G. A. Garcia, and I. Powis, Valence shell one-photon photoelectron circular dichroism in chiral systems, *Journal of Electron Spectroscopy and Related Phenomena* **204**, 322 (2015).
 - [7] M. H. M. Janssen and I. Powis, Detecting chirality in molecules by imaging photoelectron circular dichroism, *Phys. Chem. Chem. Phys.* **16**, 856 (2014).
 - [8] C. Lux, M. Wollenhaupt, T. Bolze, Q. Liang, J. Köhler, C. Sarpe, and T. Baumert, Circular dichroism in the photoelectron angular distributions of camphor and fenchone from multiphoton ionization with femtosecond laser pulses, *Angewandte Chemie International Edition* **51**, 5001 (2012).
 - [9] C. S. Lehmann, N. B. Ram, I. Powis, and M. H. M. Janssen, Imaging photoelectron circular dichroism of chiral molecules by femtosecond multiphoton coincidence detection, *The Journal of Chemical Physics* **139**, 234307 (2013).
 - [10] S. Beaulieu, A. Ferré, R. Gêneaux, R. Canonge, D. Descamps, B. Fabre, N. Fedorov, F. Légaré, S. Petit, T. Ruchon, *et al.*, Universality of photoelectron circular dichroism in the photoionization of chiral molecules, *New Journal of Physics* **18**, 102002 (2016).
 - [11] R. Weinkauf, E. Schlag, T. Martinez, and R. Levine, Nonstationary electronic states and site-selective reactivity, *The Journal of Physical Chemistry A* **101**, 7702 (1997).
 - [12] P. B. Corkum, M. Y. Ivanov, and J. S. Wright, Subfemtosecond processes in strong laser fields, *Annual review of physical chemistry* **48**, 387 (1997).
 - [13] L. Cederbaum and J. Zobeley, Ultrafast charge migration by electron correlation, *Chemical Physics Letters* **307**, 205 (1999).
 - [14] J. Breidbach and L. S. Cederbaum, Migration of holes: Formalism, mechanisms, and illustrative applications, *The Journal of Chemical Physics* **118**, 3983 (2003).
 - [15] F. Remacle and R. D. Levine, An electronic time scale in chemistry, *Proceedings of the National Academy of Sciences* **103**, 6793 (2006), <https://www.pnas.org/content/103/18/6793.full.pdf>.
 - [16] A. I. Kuleff and L. S. Cederbaum, Ultrafast correlation-driven electron dynamics, *Journal of Physics B: Atomic, Molecular and Optical Physics* **47**, 124002 (2014).
 - [17] F. Calegari, D. Ayuso, A. Trabattoni, L. Belshaw, S. De Camillis, S. Anumula, F. Fras-

- setto, L. Poletto, A. Palacios, P. Decleva, J. B. Greenwood, F. Martín, and M. Nisoli, Ultrafast electron dynamics in phenylalanine initiated by attosecond pulses, *Science* **346**, 336 (2014), <https://science.sciencemag.org/content/346/6207/336.full.pdf>.
- [18] M. Nisoli, P. Decleva, F. Calegari, A. Palacios, and F. Martín, Attosecond electron dynamics in molecules, *Chemical Reviews* **117**, 10760 (2017), PMID: 28488433.
- [19] A. F. Ordonez and O. Smirnova, Propensity rules in photoelectron circular dichroism in chiral molecules. I. Chiral hydrogen, *Physical Review A* **99**, 043416 (2019).
- [20] W. Yao, D. Xiao, and Q. Niu, Valley-dependent optoelectronics from inversion symmetry breaking, *Phys. Rev. B* **77**, 235406 (2008).
- [21] A. F. Ordonez and O. Smirnova, Propensity rules in photoelectron circular dichroism in chiral molecules. ii. general picture, *Physical Review A* **99**, 043417 (2019).
- [22] F. de Juan, A. G. Grushin, T. Morimoto, and J. E. Moore, Quantized circular photogalvanic effect in weyl semimetals, *Nature communications* **8**, 1 (2017).
- [23] Note that Juan et al. [22] use $\beta = -i\sigma$ to formulate Eqs.5,6.
- [24] R. G. Barrera, G. A. Estevez, and J. Giraldo, Vector spherical harmonics and their application to magneto-statics, *European Journal of Physics* **6**, 287 (1985), publisher: IOP Publishing.
- [25] S. Eckart, M. Kunitski, M. Richter, A. Hartung, J. Rist, F. Trinter, K. Fehre, N. Schlott, K. Henrichs, L. P. H. Schmidt, *et al.*, Ultrafast preparation and detection of ring currents in single atoms, *Nature Physics* **14**, 701 (2018).
- [26] I. Barth and J. Manz, Electric ring currents in atomic orbitals and magnetic fields induced by short intense circularly polarized π laser pulses, *Phys. Rev. A* **75**, 012510 (2007).
- [27] J. Guo, K.-J. Yuan, H. Lu, and A. D. Bandrauk, Spatiotemporal evolution of ultrafast magnetic-field generation in molecules with intense bichromatic circularly polarized uv laser pulses, *Phys. Rev. A* **99**, 053416 (2019).
- [28] A. Comby, S. Beaulieu, M. Boggio-Pasqua, D. Descamps, F. Légaré, L. Nahon, S. Petit, B. Pons, B. Fabre, Y. Mairesse, and V. Blanchet, Relaxation dynamics in photoexcited chiral molecules studied by time-resolved photoelectron circular dichroism: Toward chiral femtochemistry, *The Journal of Physical Chemistry Letters* **7**, 4514 (2016), PMID: 27786493.
- [29] A. F. Ordonez and O. Smirnova, Disentangling enantiosensitivity from dichroism using bichromatic fields, *arXiv:2009.03655 [physics]* (2020).
- [30] P. V. Demekhin, A. N. Artemyev, A. Kastner, and T. Baumert, Photoelectron circular dichroism with two overlapping laser pulses of carrier frequencies ω and 2ω linearly polarized in two mutually orthogonal

- directions, Phys. Rev. Lett. **121**, 253201 (2018).
- [31] P. V. Demekhin, Photoelectron circular dichroism with Lissajous-type bichromatic fields: One-photon versus two-photon ionization of chiral molecules, Physical Review A **99**, 063406 (2019).
- [32] S. Rozen, A. Comby, E. Bloch, S. Beauvarlet, D. Descamps, B. Fabre, S. Petit, V. Blanchet, B. Pons, N. Dudovich, and Y. Mairesse, Controlling subcycle optical chirality in the photoionization of chiral molecules, Phys. Rev. X **9**, 031004 (2019).
- [33] We consider transform limited pulses.
- [34] D. Toffoli, M. Stener, G. Fronzoni, and P. Decleva, Convergence of the multicenter b-spline dft approach for the continuum, Chemical Physics **276**, 25 (2002).
- [35] S. Turchini, N. Zema, G. Contini, G. Alberti, M. Alagia, S. Stranges, G. Fronzoni, M. Stener, P. Decleva, and T. Prosperi, Circular dichroism in photoelectron spectroscopy of free chiral molecules: Experiment and theory on methyl-oxirane, Phys. Rev. A **70**, 014502 (2004).
- [36] M. Stener, G. Fronzoni, D. D. Tommaso, and P. Decleva, Density functional study on the circular dichroism of photoelectron angular distribution from chiral derivatives of oxirane, The Journal of Chemical Physics **120**, 3284 (2004).
- [37] S. Stranges, S. Turchini, M. Alagia, G. Alberti, G. Contini, P. Decleva, G. Fronzoni, M. Stener, N. Zema, and T. Prosperi, Valence photoionization dynamics in circular dichroism of chiral free molecules: The methyl-oxirane, The Journal of Chemical Physics **122**, 244303 (2005).
- [38] D. Di Tommaso, M. Stener, G. Fronzoni, and P. Decleva, Conformational effects on circular dichroism in the photoelectron angular distribution, ChemPhysChem **7**, 924 (2006).
- [39] S. Turchini, D. Catone, G. Contini, N. Zema, S. Irrera, M. Stener, D. Di Tommaso, P. Decleva, and T. Prosperi, Conformational effects in photoelectron circular dichroism of alaninol, ChemPhysChem **10**, 1839 (2009).
- [40] This can be shown by noting that \vec{j}_{12} depends on the product of the transition amplitudes to states $|1\rangle$ and $|2\rangle$.
- [41] S. Beaulieu, A. Comby, D. Descamps, B. Fabre, G. A. Garcia, R. Géneaux, A. G. Harvey, F. Légaré, Z. Mašín, L. Nahon, A. F. Ordonez, S. Petit, B. Pons, Y. Mairesse, O. Smirnova, and V. Blanchet, Photoexcitation circular dichroism in chiral molecules, Nature Physics **14**, 484 (2018).
- [42] A. F. Ordonez and O. Smirnova, In preparation.
- [43] Y.-I. Suzuki, Communication: Photoionization of degenerate orbitals for randomly oriented molecules: The effect of time-reversal symmetry on recoil-ion momentum angular distributions, The Journal of chemical physics **148**, 151101 (2018).

- [44] J. J. Sakurai and E. D. Commins, Modern quantum mechanics, revised edition (1995).
- [45] A. F. Ordonez and O. Smirnova, Generalized perspective on chiral measurements without magnetic interactions, Physical Review A **98**, 063428 (2018).
- [46] We define the Fourier transform as $\vec{\tilde{E}}(\omega) = \int_{-\infty}^{\infty} \vec{E}(t) e^{i\omega t} dt$ and assume $\vec{\tilde{E}}(\omega) = \mathcal{E}(\omega)(\vec{x} - i\sigma\vec{y})/\sqrt{2}$ at the transition frequency.
- [47] A. F. Ordonez and O. Smirnova, On the molecular information revealed by photoelectron angular distributions of isotropic samples, arXiv:2009.03660 [physics] (2020).